IET Communications

Research Article

Physical layer security performance analysis of the time reversal transmission system

ISSN 1751-8628
Received on 30th August 2019
Revised 13th November 2019
Accepted on 20th November 2019
E-First on 29th January 2020
doi: 10.1049/iet-com.2019.0872
www.ietdl.org

Weijia Lei[1], *Miaomiao Yang*[1] ✉, *Li Yao*[1], *Hongjiang Lei*[1]
[1]*School of Communication and Information Engineering, Chongqing University of Posts and Telecommunications, Chongqing 400065, People's Republic of China*
✉ *E-mail: yangmiao1004@163.com*

Abstract: Thanks to its characteristics of temporal compression and spatial focusing, the time reversal (TR) transmission system has the intrinsic capability of anti-eavesdropping. This study analyses the physical layer security performance of the TR transmission system. The probability density functions and cumulative distribution functions of the signal-to-noise ratio of the legitimate user and eavesdropper are given. On this basis, the theoretical expressions of the ergodic capacities of the legitimate channel and the wiretap channel, and the achievable ergodic secrecy rate are derived. The bit error rates of the legitimate user and eavesdropper for binary phase-shift keying modulation are given too. The correctness of the theoretical derivation is verified by simulation. For the legitimate user, the signal power increases as the number of paths increases, which indicates a higher diversity gain can be obtained, and the inter-symbol interference power decreases as the up-sampling factor increases. So, the signal-to-interference-plus-noise ratio (SINR) of the received signal can be significantly improved by appropriately reducing the spectral efficiency. However, the received signal's SINR of the eavesdropper cannot be promoted obviously. That is to say, compared with the eavesdropper, the legitimate user can achieve a higher rate and a lower BER, so secure transmission can be realised.

1 Introduction

1.1 background and related works

Time reversal (TR) transmission technology, which takes the time-reversed and conjugated impulse response of the channel as a pre-filter at the transmitter, exploits the multipath radio propagation environment and focuses the signal energy on the desired time and space target [1–4]. When the bandwidth is large enough, a large number of multiple paths naturally exist in the scattering environment and can be utilised to form virtual multiple transmission antennas by the TR pre-processing at the transmitter [5]. As the bandwidth increases, the sampling period of the signal decreases, so the paths with a smaller delay gap can be identified. The broader is the bandwidth, the more paths can be utilised in the TR system. The TR technique was originally designed for acoustics and ultrasound applications [6, 7]. In the last decade, the applications of the TR technique in other fields have been researched, such as wireless communications [8, 9], high-resolution imaging [10], indoor positioning [11], spatial filed shaping [12] etc. Thanks to the spatial–temporal focusing effect of the TR technique, the signal energy at the target receiver can be improved. The performance of the TR technology is analysed in a broadband communication system [13], and the results show that the received signal energy can be enhanced while the interference is effectively suppressed by using TR technology. The concept of time-reversal division multiple access (TRDMA) [14] has been proposed in multi-user downlink communication systems, the expression of the average signal-to-interference-plus-noise ratio (SINR) is derived, and the simulation results of the achievable sum rate and outage probability are given. In [15], we have derived the probability density function (PDF) and cumulative distribution function (CDF) of the signal-to-noise ratio (SNR) at the receiver in a TR communication system and obtained the ergodic capacity and outage probability based on the PDF.

Information security is an important issue of communications. Owing to the broadcast nature of wireless communication systems, reliability and security face serious challenges. Wyner showed that when an eavesdropper's channel is a degraded version of the main channel, secure transmission of information can be achieved from the source to the destination by using technologies in the physical layer [16]. Although the openness of wireless channels poses a serious challenge to secure transmission, however, using its random fading characteristic is an effective way to achieve secure transmission of information based on Wyner's theory. In [17], the physical layer security (PLS) is studied in a multi-user massive multiple-input multiple-output (MIMO) system with imperfect channel state information. By using the proposed channel scheme, the system's secrecy performance is improved. Zhang *et al*. [18] proposed a secrecy-based access control scheme and a merge-and-split-based coalition formation algorithm to improve the performance of the PLS in the device-to-device communications.

The spatial focusing effect of the TR technology reduces the signal leakage to unintended receivers and improves the received signal's quality at the target receiver, so it has an intrinsic anti-eavesdropping property and is an effective technology to achieve PLS. The achievable secrecy rates are simulated in [19] when the TR or maximum ratio transmission pre-filter is employed in a multiple-input-single-output (MISO) orthogonal frequency division multiplexing system. The simulation results show that a higher secrecy rate can be achieved when the TR pre-filter is employed. The PLS performance of a MIMO ultra-wideband (UWB) system adopting TR pre-processing is studied in [20]. The simulation results show that the secrecy rate can be significantly promoted by the application of TR technology. In [21], the secrecy capacity of a TR transmission system is simulated for both the specular radio channel and the dense diffuse scattering radio channel. Simulation results show that the security performance increases with the increase of the SNR and then comes to a ceiling in the specular channel, while it increases continuously with the increase of SNR in the diffuse radio channel. Tran *et al*. [22] proposed the term effective secrecy SINR and used it to measure the PLS performance of the system. The mean of the secrecy SINR has been derived when the legitimate channel and the wiretap channel are correlative or the transmitting antennas are correlative with each other. The results of analysis and simulation indicate that the correlations lead to the decline of security performance. The SNR of the target and unintended receivers is analysed in a distributed TR (DTR) transmission system in [23]. The results show that DTR

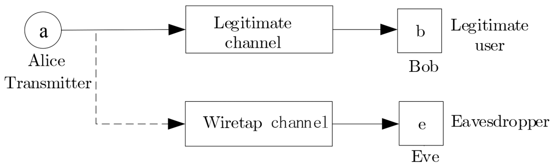

Fig. 1 *Channel model*

transmission can effectively concentrate the signal energy at the desired receiver, so the SNR of the undesired receiver is significantly lower than that of the desired receiver and PLS transmission can be realised. An artificial noise (AN) method was proposed to enhance the security performance of the TR transmission system in [24], and the closed-form expressions of the average values of SNR of the legitimate user and the eavesdropper were derived. Also, an approximate closed-form secrecy rate was derived too. The simulation results show that AN with small power can significantly improve the security performance of the system. In [25], the TR technique was applied to simultaneous wireless information and power transfer network in the presence of an active eavesdropper over the frequency-selective fading channel, and a moment generating function-based method was presented to derive the average symbol error rate (SER). The results indicate that the TR technique efficiently improved the SER performance of the legitimate user. Comprehensive performance analysis of multi-user MISO UWB systems with a TR pre-filter is provided in [26]. The theoretical expression of average SINR is derived, and the simulation results of the channel capacity and bit error rate (BER) are given. These results show that the high-spatial correlation and channel estimation errors can cause a remarkable reduction in bandwidth efficiency. In [27], the approximate closed expression of the inter-symbol interference (ISI) power is derived in a TR system, and spatial focusing and time compression performance of the TR beamforming are analysed. An equalised TR technology has been proposed, which mitigates ISI and can obtain a better BER performance.

Since the transmitting signal is pre-processed by a TR filter, and the received signal in the TR transmission system is a superposition of the signals which come from the multiple paths and are correlative to each other, the analysis of the TR system's performance is very complicated. So far, only the average values (or expectations) of the received SNR of some TR transmission systems have been analysed, including the mean values of SNR and SINR of the target receiver and the unintended receiver [5, 14, 22–24, 26]. The average values of the system rate or capacity are obtained through simulation [2, 5, 14]. We have derived the average values of the capacity in [15]. In the case where eavesdroppers exist, however, the relevant works only give the instantaneous value of the achievable secrecy rate of the TR system [19–21], not the expectation of it.

1.2 Motivation and contributions

There are several PLS solutions in secure wireless transmission, such as signal alignment, beamforming, AN injection, and cooperative jamming. However, signal alignment and beamforming can only be used in multi-antenna systems. The AN schemes (including cooperative jamming) are usually employed in multi-antenna systems, and their performance will degrade seriously in single transmitting antenna systems. However, by using TR technology, a better PLS performance can be achieved in single-antenna systems. This study analyses the PLS performance of the TR systems over the Rayleigh fading channels.

- Firstly, the PDF and CDF of the SNR at the eavesdropper (unintended receiver) are derived. At the eavesdropper, the SNR concentrates in a lower region, and it only has a slight shift when the number of paths is doubled. This means that the eavesdropper cannot benefit from the TR pre-processing. On the contrary, at the legitimate user, the SNR concentrates in a higher region, and the larger the number of paths is, the higher the concentrated region is. This means that the legitimate user can obtain diversity gain from the TR pre-processing, and the larger the number of paths is, the higher the diversity gain is.
- Based on the work of Lei and Yao [15], in which the PDF and CDF of the SNR at the legitimate user (target receiver) are given, we further derive the expressions of the ergodic capacities of the legitimate channel, the wiretap channel, and the ergodic achievable secrecy rate. The achievable secrecy rate is an important metric of PLS, which can provide theoretical guidance for the research of the PLS mechanism. Both the ergodic capacities of the legitimate channel and the wiretap channel grow with the increase of the transmission power. The former has a larger value and a higher increasing rate than those of the latter. As a result, a non-zero achievable secrecy rate can be obtained, and it grows as the transmission power increases. Owing to the constraint of ISI, the capacities of both the legitimate channel and the wiretap channel have their upper bounds, so has an achievable secrecy rate. These bounds increase as the up-sampling factor D increases because the ISI power decreases. These bounds also increase with the increase in the number of paths, since the signal power increases. Compared with direct transmission (DT) systems, where only a very small secrecy rate can be achieved even if the transmission power approaches infinity, TR systems have a better PLS performance.
- We also give the average BERs of the legitimate user and the eavesdropper when binary phase-shift keying (BPSK) modulation is used. As the transmission power increases, the BER of the legitimate user decreases rapidly while that of the eavesdropper decreases slowly. The larger the number of paths is or the higher the up-sampling factor D is, the more quickly the BER of the legitimate user drops, while that of the eavesdropper always declines slowly.
- Different from [24], which only gave an approximate closed-form average secrecy rate by using Jenson inequality, the PDFs of received SNR of the legitimate user and the eavesdropper are derived in this study. Based on the PDFs, a more accurate average secrecy rate and other PLS performance can be further deduced.

The rest of this paper is organised as follows. Section 2 introduces the system model. In Section 3, secure performance is investigated. The simulation results are presented and discussed in Section 4. Finally, Section 5 concludes the paper.

2 System model

The channel model is shown in Fig. 1. It includes a transmitter (Alice), a legitimate user (Bob), and an eavesdropper (Eve), which are abbreviated as a, b, and e. We assume that the channel noise is additive white Gaussian noise (AWGN). Both the legitimate channel and the wiretap channel are multipath fading channels, and the two channels are independent of each other. The paths of each channel are also independent of each other. The discrete time channel impulse response (CIR) of the two channels can be expressed as

$$h_m[n] = \sum_{l=0}^{L_m-1} h_{m,l}\delta[n-l], \tag{1}$$

where $m \in \{\mathrm{b}, \mathrm{e}\}$ represents the channel from Alice to Bob or Eve, L_m is the number of channel m's paths and $\delta[\cdot]$ is the Dirac delta function. $h_{m,l}$is the fading coefficient of the lth path of channel m, i.e. the coefficient of the lth tap of the CIR. $h_{m,l}$ is a circularly symmetric complex Gaussian random variable with zero mean and

$$E\left[\left|h_{m,l}\right|^2\right] = \eta_m \mathrm{e}^{-(lT_\mathrm{s}/\sigma_\mathrm{T})} = \sigma_{m,l}^2, \quad 0 \le l \le L_m - 1, \tag{2}$$

where $E[\cdot]$ represents the expectation operation, T_s is the sampling period, σ_T is the delay spread of the channel, $\mathrm{e}^{-(lT_\mathrm{s}/\sigma_\mathrm{T})}$ is the smallscale fading coefficient of the lth path, and η_m is the large-scale fading coefficient of the channel m.

The procedure of the TR transmission consists of two steps. The target receiver (Bob) firstly sends a pilot signal to Alice. Alice estimates the CIR of the channel, pre-filters the transmitting signals, and sends them to Bob. The impulse response of the filter is the time-reversed and conjugate version of the normalised CIR of the legitimate channel, i.e.

$$g[n] = \frac{h_{\mathrm{b}}^{*}[L_{\mathrm{b}} - 1 - n]}{\sqrt{\sum_{l=0}^{L_{\mathrm{b}}-1} \left|h_{\mathrm{b},l}\right|^{2}}} = G h_{\mathrm{b}}^{*}[L_{\mathrm{b}} - 1 - n], \tag{3}$$

where the superscript '$*$' represents conjugation and $G = \left(\sum_{l=0}^{L_{\mathrm{b}}-1} |h_{\mathrm{b},l}|^{2}\right)^{-(1/2)}$ is the normalisation factor. This pre-processing filter can be taken as a part of the equivalent channel of the system, so the equivalent CIRs of the legitimate channel and the wiretap channel can be written, respectively, as

(see (4))

(see (5))

where '$*$' denotes the convolution operation, $L_1 = \min(L_{\mathrm{b}}, L_{\mathrm{e}})$ and $L_2 = \max(L_{\mathrm{b}}, L_{\mathrm{e}})$.

The sequence of information symbols is denoted as $X[k]$. $X[k]$ is interpolated to increase the sampling rate to $1/T_{\mathrm{s}}$ (up-sampling), where the up-sampling factor D is the ratio of the sampling rate to the symbol rate. The up-sampled signal sequence $x[n]$ is given as

$$x[n] = \begin{cases} X[k], & \mathrm{if} n = kD. \\ 0, & \mathrm{else}. \end{cases} \tag{6}$$

Let the power of the transmitted signal be P_X. The up-sampled signal sequence passes through the pre-processing filter and the multipath channels. The received signals of Bob and Eve can be expressed as

$$\begin{aligned} y_m[n] &= (x * h_{m,\mathrm{eq}})[n] + z_m[n] \\ &= (x * g * h_m)[n] + z_m[n], \end{aligned} \tag{7}$$

where $z_m[n]$ is the AWGN with zero mean and variance σ_m^2.

For simplicity, $(L_m - 1)$ $(m \in \{\mathrm{b}, \mathrm{e}\})$ is assumed to be a multiple of D. Bob and Eve, respectively, extract (down-sample) the received signal, and take the samples with the index of an integer multiple of D as the received symbol samples. Thus, the sequences of sampled symbols of Bob and Eve are given as

$$\begin{aligned} Y_m[k] &= y_m[kD] \\ &= \sum_{i=0}^{(L_m + L_{\mathrm{b}} - 2)/D} h_{m,\mathrm{eq}}[Di] X[k - i] + Z_m[k] \\ &= \underbrace{h_{m,\mathrm{eq}}[L_{\mathrm{b}} - 1] X\left[k - \frac{L_{\mathrm{b}} - 1}{D}\right]}_{\text{signal}} \\ &\quad \underbrace{+ \sum_{\substack{i=0 \\ i \neq (L_{\mathrm{b}} - 1)/D}}^{(L_m + L_{\mathrm{b}} - 2)/D} h_{m,\mathrm{eq}}[Di] X[k - i]}_{\text{ISI}} + \underbrace{Z_m[k]}_{\text{noise}}, \end{aligned} \tag{8}$$

where $Z_m[k] = z_m[kD]$ is the sample of channel noise. The first part on the right-hand side of the last equal of (8) is the signal and the second part is ISI.

3 Performance analysis

According to (8), the powers of the signal and ISI of the received signals of Bob can be expressed as

$$\begin{aligned} P_{\mathrm{b}}^{\mathrm{sig}} &= \left|h_{\mathrm{b},\mathrm{eq}}[L_{\mathrm{b}} - 1] X\left[k - \frac{L_{\mathrm{b}} - 1}{D}\right]\right|^{2} \\ &= P_X\left(\sum_{l=0}^{L_{\mathrm{b}} - 1} \left|h_{b,l}\right|^{2}\right), \end{aligned} \tag{9}$$

$$\begin{aligned} P_{\mathrm{b}}^{\mathrm{ISI}} &= \sum_{\substack{i=0 \\ i \neq (L_{\mathrm{b}} - 1)/D}}^{(2L_{\mathrm{b}} - 2)/D} \left|h_{\mathrm{b},\mathrm{eq}}[Di] X[k - i]\right|^{2} \\ &= 2G^{2} P_X \sum_{i=0}^{(L_{\mathrm{b}} - 1)/D - 1} \left|\sum_{l=0}^{Di} h_{b,l} h_{b,L_{\mathrm{b}} - 1 - Di + l}^{*}\right|^{2}. \end{aligned} \tag{10}$$

Similarly, the power of the signal and ISI of the received signals of Eve are derived as

$$\begin{aligned} P_{\mathrm{e}}^{\mathrm{sig}} &= \left|h_{\mathrm{e},\mathrm{eq}}[L_{\mathrm{b}} - 1] X\left[k - \frac{L_{\mathrm{b}} - 1}{D}\right]\right|^{2} \\ &= G^{2} P_X \left|\sum_{l=0}^{L_1 - 1} h_{e,l} h_{b,l}^{*}\right|^{2}, \end{aligned} \tag{11}$$

$$\begin{aligned} h_{\mathrm{b},eq}[n] &= (g * h_{\mathrm{b}})[n] \\ &= \begin{cases} G \sum_{l=0}^{n} h_{\mathrm{b},l} h_{b,L_{\mathrm{b}} - 1 - n + l}^{*}, & n = 0, 1, \ldots, L_{\mathrm{b}} - 1, \\ G \sum_{l=n-L_{\mathrm{b}}+1}^{L_{\mathrm{b}} - 1} h_{\mathrm{b},l} h_{b,L_{\mathrm{b}} - 1 - n + l}^{*}, & n = L_{\mathrm{b}}, L_{\mathrm{b}} + 1, \ldots, 2L_{\mathrm{b}} - 2, \end{cases} \end{aligned} \tag{4}$$

$$\begin{aligned} h_{\mathrm{e},eq}[n] &= (g * h_{\mathrm{e}})[n] \\ &= \begin{cases} G \sum_{l=0}^{n} h_{\mathrm{e},l} h_{b,L_{\mathrm{b}} - 1 - n + l}^{*}, & n = 0, 1, \ldots, L_1 - 1, \\ G \sum_{l=0}^{L_1 - 1} h_{\mathrm{e},n - L_{\mathrm{b}} + 1 + l} h_{b,l}^{*}, & n = L_1, L_1 + 1, \ldots, L_2 - 1, \\ G \sum_{l=n-L_{\mathrm{b}}+1}^{L_{\mathrm{e}} - 1} h_{\mathrm{e},l} h_{b,L_{\mathrm{b}} - 1 - n + l}^{*}, & n = L_2, L_2 + 1, \ldots, L_{\mathrm{e}} + L_{\mathrm{b}} - 2, \end{cases} \end{aligned} \tag{5}$$

$$P_{\mathrm{e}}^{\mathrm{ISI}} = \sum_{i=0, i \neq (L_{\mathrm{b}}-1)/D}^{(L_{\mathrm{e}}+L_{\mathrm{b}}-2)/D} \left| h_{\mathrm{e,eq}}[Di]X[k-i] \right|^2$$

$$= G^2 P_X \times \left(\sum_{i=0}^{(L_1-1)/D} \left| \sum_{l=0}^{Di} h_{\mathrm{e},l} h_{b,L_{\mathrm{b}}-1-Di+l}^{*} \right|^2 \right.$$

$$+ \sum_{i=(L_1-1)/D+1}^{(L_2-1)/D} \left| \sum_{l=0}^{L_1-1} h_{\mathrm{e},Di-L_{\mathrm{b}}+1+l} h_{b,l}^{*} \right|^2 \tag{12}$$

$$\left. + \sum_{i=(L_2-1)/D+1}^{(L_{\mathrm{e}}+L_{\mathrm{b}}-2)/D} \left| \sum_{l=Di-L_b+1}^{L_e-1} h_{\mathrm{e},l} h_{b,L_{\mathrm{b}}-1-Di+l}^{*} \right|^2 \right) - P_{\mathrm{e}}^{\mathrm{sig}}.$$

As can be seen from (10) and (12), the expressions of the ISI powers of Bob and Eve are very complicated. To get ISI powers, the sum of multiple products of two random variables should be obtained and the squares of the sums are accumulated. Furthermore, the random variables in the expressions are not mutually independent. Therefore, it is impossible to derive the analytical expressions of the PDFs of the ISI powers of Bob and Eve. However, as the up-sampling factor D increases, the number of summed items of ISI is reduced, resulting in a power decrease of ISI. When D is large enough, the ISI powers of Bob and Eve are very small compared with their noise powers and thus they can be neglected. In fact, it can be found from the simulation results of Section 4 that when D is large enough, the performance deviation caused by the ignoring of ISI is small. Therefore, similar to the works of performance analysis of TR systems [13, 19–21, 23, 24, 28], we ignore ISI and focus on the analysis of SNR.

3.1 Probability distribution of SNR of Bob

For the convenience of discussion, we give the PDF of the received SNR of Bob here again, which are derived in [15]. The received SNR of Bob is expressed as

$$\Gamma_{\mathrm{b}} = \frac{P_{\mathrm{b}}^{\mathrm{sig}}}{P_{\mathrm{b}}^{noise}} = \frac{P_X}{\sigma_{\mathrm{b}}^2} \left(\sum_{l=0}^{L_{\mathrm{b}}-1} \left| h_{b,l} \right|^2 \right) = \frac{P_X}{\sigma_{\mathrm{b}}^2} \sum_{l=0}^{L_{\mathrm{b}}-1} U_l, \tag{13}$$

where $U_l = |h_{b,l}|^2 (l = 0, 1, \ldots L_{\mathrm{b}} - 1)$.

According to [29], U_l obeys the exponential distribution for all ls, whose PDFs can be represented as

$$f_{U_l}(u_l) = \frac{1}{\sigma_{b,l}^2} \exp\left(-\frac{u_l}{\sigma_{b,l}^2} \right). \tag{14}$$

The characteristic functions (CFs) of U_l are given as

$$\psi_{U_l}(\omega) = \int_{-\infty}^{\infty} \mathrm{e}^{\mathrm{j}\omega u_l} f_{U_l}(u_l)\, \mathrm{d}u_l = \frac{1}{1 - \mathrm{j}\omega\sigma_{b,l}^2}. \tag{15}$$

Let $V = \sum_{l=0}^{L_{\mathrm{b}}-1} U_l$. As the CF of the sum of multiple independent random variables is the product of the CFs of each random variable [30], the CF of V can be obtained as

$$\psi_V(\omega) = \prod_{l=0}^{L_{\mathrm{b}}-1} \psi_{U_l}(\omega) = \prod_{l=0}^{L_{\mathrm{b}}-1} \frac{1}{1 - \mathrm{j}\omega\sigma_{b,l}^2}. \tag{16}$$

By using partial fractional expansion, we can get

$$\psi_V(\omega) = \sum_{l=0}^{L_{\mathrm{b}}-1} \frac{K_l}{1 - \mathrm{j}\omega\sigma_{b,l}^2}, \tag{17}$$

where $K_l = \prod_{j=0, j\neq l}^{L_{\mathrm{b}}-1} \sigma_{b,l}^2 / (\sigma_{b,l}^2 - \sigma_{b,j}^2)$. Furthermore, the PDF of V can be obtained as

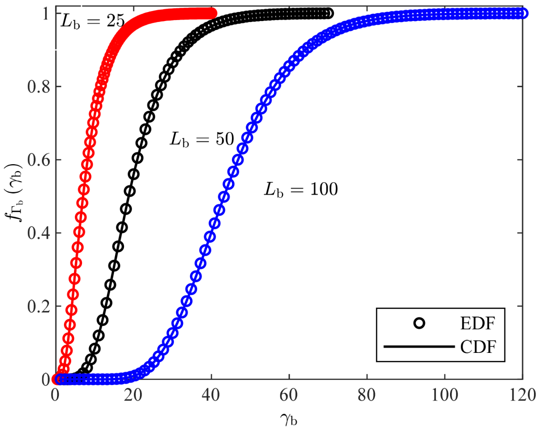

Fig. 2 *CDF of SNR of Bob*

$$f_V(v) = \frac{1}{2\pi} \int_{-\infty}^{\infty} \psi_V(\omega)\, \mathrm{e}^{-\mathrm{j}\omega t}\, \mathrm{d}\omega$$

$$= \sum_{l=0}^{L_{\mathrm{b}}-1} \frac{K_l}{\sigma_{b,l}^2} \exp\left(-\frac{v}{\sigma_{b,l}^2} \right). \tag{18}$$

The PDF of the received SNR of $\Gamma_{\mathrm{b}} = (P_X / \sigma_{\mathrm{b}}^2)V$ is derived as

$$f_{\Gamma_{\mathrm{b}}}(\gamma_{\mathrm{b}}) = f_V\left(\frac{\sigma_{\mathrm{b}}^2}{P_X} \gamma_{\mathrm{b}} \right) \frac{\sigma_{\mathrm{b}}^2}{P_X}$$

$$= \sum_{l=0}^{L_{\mathrm{b}}-1} \frac{\sigma_{\mathrm{b}}^2 K_l}{P_X \sigma_{b,l}^2} \exp\left(-\frac{\sigma_{\mathrm{b}}^2}{P_X \sigma_{b,l}^2} \gamma_{\mathrm{b}} \right). \tag{19}$$

The CDF of Γ_{b} is given as

$$F_{\Gamma_{\mathrm{b}}}(\gamma_{\mathrm{b}}) = \sum_{l=0}^{L_{\mathrm{b}}-1} K_l \left[1 - \exp\left(-\frac{\sigma_{\mathrm{b}}^2}{P_X \sigma_{\mathrm{b},l}^2} \gamma_{\mathrm{b}} \right) \right]. \tag{20}$$

Next, the correction of the derived CDF of the received SNR of Bob is verified through simulation. The CDF curves under three numbers of paths are simulated separately. The main parameters are set as follows: the bandwidth is $B = 100$, 50 or 25 MHz; the sampling period is $T_{\mathrm{s}} = 1/B$; correspondingly, the number of paths is $L_{\mathrm{b}} = 100$, 50 or 25, and the up-sampling factor D is 50, 25 or 12; the delay spread of the legitimate channel is $\sigma_{\mathrm{T}} = 500$ ns; the fading coefficient of each path follows a complex Gaussian distribution with zero mean and the variance is shown in (2); the large-scale fading coefficient is calculated according to $\eta = \eta_{\mathrm{b}} = \eta_{\mathrm{e}} = \eta_0 (d/d_0)^{-c}$, where $d_0 = 10$ m is the reference distance, $d = 100$ m is the distance between Alice and Bob, $\eta_0 = 10^{-5}$ is the loss at the reference distance, and $c = 4$ is the path loss exponent. So the large-scale fading factor is $\eta = 10^{-9}$. The signal power is $P_X = 10$ mW and the noise power is -120 dBW. Fig. 2 shows the CDFs of the received SNR of Bob obtained, respectively, by simulation and the theoretical calculation according to (20). We take the Kolmogorov–Smirnov (K–S) test to evaluate the correctness and accuracy of the derived distribution. The significance level is set to 0.05, and the sample size is 10^6. The corresponding test threshold is 1.4×10^{-3}. The K–S statistic is the maximum distance between the empirical distribution function (EDF) of the sample and the theoretical CDF. The K–S statistic is 8.6514×10^{-4} when $L_{\mathrm{b}} = 100$, it is 1.3×10^{-3} when $L_{\mathrm{b}} = 50$, and it is 8.3936×10^{-4} when $L_{\mathrm{b}} = 25$. Those K–S statistics are lower than the threshold, so the hypothesis that the EDF and the theoretical CDF are identical is acceptable. This means that the derived PDF and CDF expressions are correct. The CDFs show that although the transmission power is the same, the more the number of paths is, the higher the value region the SNR concentrates distributed in. This means that the diversity gain can be obtained by TR pre-processing, and the larger the number of paths is, the higher diversity gain can be obtained.

3.2 Probability distribution of SNR of Eve

The received SNR of Eve can be expressed as

$$\Gamma_{\mathrm{e}} = \frac{P_{\mathrm{e}}^{\mathrm{sig}}}{P_{\mathrm{e}}^{\mathrm{noise}}} = \frac{P_X}{\sigma_{\mathrm{e}}^2}\left| G\sum_{l=0}^{L_1-1} h_{e,l}h_{b,l}^{*}\right|^2 . \tag{21}$$

Rewrite (21) as

$$\begin{aligned}\Gamma_{\mathrm{e}} &= \frac{P_X}{\sigma_{\mathrm{e}}^2}\left| G\sum_{l=0}^{L_1-1} h_{e,l}h_{b,l}^{*}\right|^2\\ &= \frac{P_X}{\sigma_{\mathrm{e}}^2}\left| G\sum_{l=0}^{L_1-1}\left(\mathrm{Re}[h_{e,l}h_{b,l}^{*}] + \mathrm{j}\cdot\mathrm{Im}[h_{e,l}h_{b,l}^{*}]\right)\right|^2\\ &= \frac{P_X}{\sigma_{\mathrm{e}}^2}\left| G\sum_{l=0}^{L_1-1}\left(h_{\mathrm{e},l}^{(\mathrm{r})}h_{b,l}^{(\mathrm{r})} + h_{\mathrm{e},l}^{(\mathrm{i})}h_{\mathrm{b},l}^{(\mathrm{i})}\right)\right.\\ &\quad \left. +\mathrm{j}\cdot G\sum_{l=0}^{L_1-1}\left(h_{\mathrm{e},l}^{(\mathrm{i})}h_{b,l}^{(\mathrm{r})} - h_{\mathrm{e},l}^{(\mathrm{r})}h_{\mathrm{b},l}^{(\mathrm{i})}\right)\right|^2\\ &= \frac{P_X}{\sigma_{\mathrm{e}}^2}|R + \mathrm{j}\cdot Q|^2,\end{aligned} \tag{22}$$

where $R = G\sum_{l=0}^{L_1-1}\left(h_{\mathrm{e},l}^{(\mathrm{r})}h_{b,l}^{(\mathrm{r})} + h_{\mathrm{e},l}^{(\mathrm{i})}h_{\mathrm{b},l}^{(\mathrm{i})}\right)$, $Q = G\sum_{l=0}^{L_1-1}\left(h_{\mathrm{e},l}^{(\mathrm{i})}h_{b,l}^{(\mathrm{r})} - h_{\mathrm{e},l}^{(\mathrm{r})}h_{\mathrm{b},l}^{(\mathrm{i})}\right)$, $h_{m,l}^{(\mathrm{r})}, h_{m,l}^{(\mathrm{i})}$ are the real and imaginary parts of $h_{m,l}$, respectively, $\mathrm{Re}[\cdot]$ and $\mathrm{Im}[\cdot]$ represent the operations of getting the real part and imaginary part, respectively. $h_{m,l}^{(\mathrm{r})}$ and $h_{m,l}^{(\mathrm{i})}$ are i.i.d. Gaussian random variables with zero mean and variance $\sigma_{m,l}^2/2$, hence R and Q are identically distributed random variables too. Since Γ_{e} is the result of multiple addition and multiplication of random variables which are not all independent of each other, it is impossible to get the exact PDF of Γ_{e}. According to the central limit theorem, it is feasible to take R and Q as Gaussian random variables when L is large enough. The expectation of R is given as

$$\begin{aligned}E[R] &= E\left[G\sum_{l=0}^{L_1-1}\left(h_{\mathrm{e},l}^{(\mathrm{r})}h_{b,l}^{(\mathrm{r})} + h_{\mathrm{e},l}^{(\mathrm{i})}h_{\mathrm{b},l}^{(\mathrm{i})}\right)\right]\\ &= E\left[\frac{\sum_{l=0}^{L_1-1}\left(h_{\mathrm{e},l}^{(\mathrm{r})}h_{b,l}^{(\mathrm{r})} + h_{\mathrm{e},l}^{(\mathrm{i})}h_{\mathrm{b},l}^{(\mathrm{i})}\right)}{\sqrt{\sum_{l=0}^{L_{\mathrm{b}}-1}\left|h_{\mathrm{b},l}\right|^2}}\right].\end{aligned} \tag{23}$$

The numerator and denominator of (23) are not independent, and both of them involve the sum of multiple random variables, so it is difficult to obtain the closed-form expression of (23). According to [31], the expectation of a ratio of two random variables that are not independent of each other equals to the ratio of the expectations of the two random variables plus a series expansion summation. Similar to [22], we omit the series expansion summation, so the expectation of R can be approximately treated as the ratio of the numerator's expectation to the denominator's expectation of (23), i.e.

$$\begin{aligned}E[R] &\simeq \frac{E\left[\sum_{l=0}^{L_1-1}\left(h_{\mathrm{e},l}^{(\mathrm{r})}h_{b,l}^{(\mathrm{r})} + h_{\mathrm{e},l}^{(\mathrm{i})}h_{\mathrm{b},l}^{(\mathrm{i})}\right)\right]}{E\left[\sqrt{\sum_{l=0}^{L_{\mathrm{b}}-1}\left|h_{\mathrm{b},l}\right|^2}\right]}\\ &= \frac{\sum_{l=0}^{L_1-1}\left(E\left[h_{\mathrm{e},l}^{(\mathrm{r})}h_{b,l}^{(\mathrm{r})}\right] + E\left[h_{\mathrm{e},l}^{(\mathrm{i})}h_{\mathrm{b},l}^{(\mathrm{i})}\right]\right)}{E\left[\sqrt{\sum_{l=0}^{L_{\mathrm{b}}-1}\left[\left|h_{b,l}\right|^2\right]}\right]}\\ &= 0.\end{aligned} \tag{24}$$

Similarly, the variance of R is obtained as (see (25)) . The mean and variance of Q are the same as those of R. R and Q are approximate Gaussian random variables with zero mean and variance σ^2. Thus $W = |R + \mathrm{j}Q|^2 = R^2 + Q^2$ is approximately subject to an exponential distribution, and its PDF is given as

$$f_W(w) = \frac{1}{2\sigma^2}\exp\left(-\frac{w}{2\sigma^2}\right). \tag{26}$$

The PDF of the received SNR $\Gamma_{\mathrm{e}} = (P_X/\sigma_{\mathrm{e}}^2)W$ can be written as

$$\begin{aligned}f_{\Gamma_{\mathrm{e}}}(\gamma_{\mathrm{e}}) &= f_W\left(\frac{\sigma_{\mathrm{e}}^2}{P_X}\gamma_{\mathrm{e}}\right)\frac{\sigma_{\mathrm{e}}^2}{P_X}\\ &= \frac{\sigma_{\mathrm{e}}^2}{2\sigma^2 P_X}\exp\left(-\frac{\sigma_{\mathrm{e}}^2}{2\sigma^2 P_X}\gamma_{\mathrm{e}}\right).\end{aligned} \tag{27}$$

The CDF of Γ_{e} can be deduced as

$$\begin{aligned}F_{\Gamma_{\mathrm{e}}}(\gamma_{\mathrm{e}}) &= \Pr\{\Gamma_{\mathrm{e}} \le \gamma_{\mathrm{e}}\}\\ &= \int_{-\infty}^{\gamma_{\mathrm{e}}} f_{\Gamma_{\mathrm{e}}}(t)\,\mathrm{d}t\\ &= \int_{-\infty}^{\gamma_{\mathrm{e}}} \frac{\sigma_{\mathrm{e}}^2}{2\sigma^2 P_X}\exp\left(\frac{\sigma_{\mathrm{e}}^2}{2\sigma^2 P_X}t\right)\mathrm{d}t\\ &= 1 - \exp\left(-\frac{\sigma_{\mathrm{e}}^2}{2\sigma^2 P_X}\gamma_{\mathrm{e}}\right).\end{aligned} \tag{28}$$

$$\begin{aligned}\sigma^2 = E\left[(R - E[R])^2\right] &= E\left[\frac{\left(\sum_{l=0}^{L_1-1}\left(h_{\mathrm{e},l}^{(\mathrm{r})}h_{b,l}^{(\mathrm{r})} + h_{\mathrm{e},l}^{(\mathrm{i})}h_{\mathrm{b},l}^{(\mathrm{i})}\right)\right)^2}{\sum_{l=0}^{L_{\mathrm{b}}-1}\left|h_{\mathrm{b},l}\right|^2}\right]\\ &\simeq \frac{E\left[\left(\sum_{l=0}^{L_1-1}\left(h_{\mathrm{e},l}^{(\mathrm{r})}h_{b,l}^{(\mathrm{r})} + h_{\mathrm{e},l}^{(\mathrm{i})}h_{\mathrm{b},l}^{(\mathrm{i})}\right)\right)^2\right]}{E\left[\sum_{l=0}^{L_{\mathrm{b}}-1}\left|h_{\mathrm{b},l}\right|^2\right]}\\ &= \frac{E\left[\sum_{l=0}^{L_1-1}\left(\left(h_{\mathrm{e},l}^{(\mathrm{r})}h_{b,l}^{(\mathrm{r})} + h_{\mathrm{e},l}^{(\mathrm{i})}h_{\mathrm{b},l}^{(\mathrm{i})}\right)^2 + 2\sum_{l_1=l+1}^{L_1-1}\left(h_{\mathrm{e},l}^{(\mathrm{r})}h_{b,l}^{(\mathrm{r})} + h_{\mathrm{e},l}^{(\mathrm{i})}h_{\mathrm{b},l}^{(\mathrm{i})}\right)\left(h_{\mathrm{e},l_1}^{(\mathrm{r})}h_{b,l_1}^{(\mathrm{r})} + h_{\mathrm{e},l_1}^{(\mathrm{i})}h_{\mathrm{b},l_1}^{(\mathrm{i})}\right)\right)\right]}{\sum_{l=0}^{L_{\mathrm{b}}-1}\sigma_{\mathrm{b},l}^2}\\ &= \frac{\sum_{l=0}^{L_1-1}E\left[\left(h_{\mathrm{e},l}^{(\mathrm{r})}h_{b,l}^{(\mathrm{r})}\right)^2 + \left(h_{\mathrm{e},l}^{(\mathrm{i})}h_{\mathrm{b},l}^{(\mathrm{i})}\right)^2 + 2h_{\mathrm{e},l}^{(\mathrm{r})}h_{b,l}^{(\mathrm{r})}h_{\mathrm{e},l}^{(\mathrm{i})}h_{\mathrm{b},l}^{(\mathrm{i})}\right]}{\sum_{l=0}^{L_{\mathrm{b}}-1}\sigma_{\mathrm{b},l}^2}\\ &= \frac{\sum_{l=0}^{L_1-1}\left(E\left[\left(h_{\mathrm{e},l}^{(\mathrm{r})}h_{b,l}^{(\mathrm{r})}\right)^2\right] + E\left[\left(h_{\mathrm{e},l}^{(\mathrm{i})}h_{\mathrm{b},l}^{(\mathrm{i})}\right)^2\right]\right)}{\sum_{l=0}^{L_{\mathrm{b}}-1}\sigma_{\mathrm{b},l}^2} = \frac{\sum_{l=0}^{L_1-1}\sigma_{\mathrm{e},l}^2\sigma_{\mathrm{b},l}^2}{2\sum_{l=0}^{L_{\mathrm{b}}-1}\sigma_{\mathrm{b},l}^2}.\end{aligned} \tag{25}$$

The accuracy of the approximate theoretic CDF of Eve's SNR is evaluated through simulation. The simulation conditions are the same as those of the simulation of CDF of legitimate user's SNR. The curves of CDF and EDF are plotted in Fig. 3. It can be seen that the theoretical CDFs deviate a little from the EDFs in the low SNR area, but they are very close in the high SNR area. The root mean square values of the difference between the simulation values and the theoretical values are, respectively, 0.0082, 0.0150, and 0.0221 for $L_{\mathrm{e}} = 100$, 50, and 25. The results show that the approximate processing in the derivation process of the probability distribution of Eve's SNR is feasible, and the larger the number of paths is, the smaller the deviation is between the approximate theoretical CDF and the EDF. Eve's CDF is generally concentrated distributed in a lower SNR region compared with that of Bob. What is more, when the number of paths increases, the CDF curve shifts right only a little. This indicates that Eve cannot obviously benefit from TR pre-filtering.

3.3 Ergodic secrecy rate

The instantaneous channel capacities of the legitimate channel and the wiretap channel are given as

$$C_m = \frac{1}{D}\log_2(1 + \gamma_m), \tag{29}$$

where C_m is the function of γ_m, and γ_m is a random variable. The ergodic capacities of the legitimate channel and the wiretap channel can be obtained, respectively, as

$$\begin{aligned}\bar{C}_{\mathrm{b}} &= E\left[\frac{1}{D}\log_2(1 + \gamma_{\mathrm{b}})\right]\\ &= \int_0^{\infty} \frac{1}{D}\log_2(1 + \gamma_{\mathrm{b}}) f_{\Gamma_{\mathrm{b}}}(\gamma_{\mathrm{b}})\,\mathrm{d}\gamma_{\mathrm{b}}\\ &= \sum_{l=0}^{L-1} \frac{\sigma_{\mathrm{b}}^2 K_l}{D P_X \sigma_{\mathrm{b},l}^2}\int_0^{\infty} \log_2(1 + \gamma_{\mathrm{b}})\exp\left(-\frac{\sigma_{\mathrm{b}}^2\gamma_{\mathrm{b}}}{P_X\sigma_{\mathrm{b},l}^2}\right)\mathrm{d}\gamma_{\mathrm{b}}\\ &= -\sum_{l=0}^{L-1} \frac{K_l}{D}\exp\left(\frac{\sigma_{\mathrm{b}}^2}{P_X\sigma_{\mathrm{b},l}^2}\right)E_{\mathrm{i}}\left(-\frac{\sigma_{\mathrm{b}}^2}{P_X\sigma_{\mathrm{b},l}^2}\right),\end{aligned} \tag{30}$$

$$\begin{aligned}\bar{C}_{\mathrm{e}} &= E\left[\frac{1}{D}\log_2(1 + \gamma_{\mathrm{e}})\right]\\ &= \int_0^{\infty} \frac{1}{D}\log_2(1 + \gamma_{\mathrm{e}}) f_{\Gamma_{\mathrm{e}}}(\gamma_{\mathrm{e}})\,\mathrm{d}\gamma_{\mathrm{e}}\\ &= \frac{\sigma_{\mathrm{e}}^2}{2D\sigma^2 P_X}\int_0^{\infty} \log_2(1 + \gamma_{\mathrm{e}})\exp\left(-\frac{\sigma_{\mathrm{e}}^2\gamma_{\mathrm{e}}}{2\sigma^2 P_X}\right)\mathrm{d}\gamma_{\mathrm{e}}\\ &= -\frac{1}{D}\exp\left(\frac{\sigma_{\mathrm{e}}^2}{2\sigma^2 P_X}\right)E_{\mathrm{i}}\left(-\frac{\sigma_{\mathrm{e}}^2}{2\sigma^2 P_X}\right),\end{aligned} \tag{31}$$

where $E_{\mathrm{i}}(t) = \int_{-\infty}^{t} (\mathrm{e}^x/x)\,\mathrm{d}x$ is the exponential integral function [32].

The instantaneous achievable secrecy rate can be expressed as

$$\begin{aligned}R_{\mathrm{s}} &= [C_{\mathrm{b}} - C_{\mathrm{e}}]^+\\ &= \begin{cases}\dfrac{1}{D}(\log_2(1 + \gamma_{\mathrm{b}}) - \log_2(1 + \gamma_{\mathrm{e}})), & \gamma_{\mathrm{b}} \ge \gamma_{\mathrm{e}}\\ 0, & \gamma_{\mathrm{b}} < \gamma_{\mathrm{e}}\end{cases},\end{aligned} \tag{32}$$

where $[x]^+ = \max[x, 0]$, i.e. the achievable secrecy rate is zero when the capacity of the wiretap channel is greater than that of the legitimate channel.

Since the legitimate channel and wiretap channel are independent of each other, the ergodic secrecy rate can be calculated as

$$\begin{aligned}\bar{R}_{\mathrm{s}} &= E[R_{\mathrm{s}}]\\ &= \int_0^{\infty}\int_0^{\infty} R_{\mathrm{s}} f_{\Gamma_{\mathrm{b}}}(\gamma_{\mathrm{b}}) \cdot f_{\Gamma_{\mathrm{e}}}(\gamma_{\mathrm{e}})\,\mathrm{d}\gamma_{\mathrm{e}}\,\mathrm{d}\gamma_{\mathrm{b}}\\ &= \int_0^{\infty}\int_0^{\gamma_{\mathrm{b}}} \left(\frac{1}{D}(\log_2(1 + \gamma_{\mathrm{b}}) - \log_2(1 + \gamma_{\mathrm{e}}))\right) f_{\Gamma_{\mathrm{b}}}(\gamma_{\mathrm{b}}) f_{\Gamma_{\mathrm{e}}}(\gamma_{\mathrm{e}})\,\mathrm{d}\gamma_{\mathrm{e}}\,\mathrm{d}\gamma_{\mathrm{b}}\\ &= \frac{1}{D\ln 2}\left[\int_0^{\infty} \ln(1 + \gamma_{\mathrm{b}}) f_{\Gamma_{\mathrm{b}}}(\gamma_{\mathrm{b}}) F_{\Gamma_{\mathrm{e}}}(\gamma_{\mathrm{b}})\,\mathrm{d}\gamma_{\mathrm{b}}\right]\\ &\quad + \frac{1}{D\ln 2}\left[\int_0^{\infty} \ln(1 + \gamma_{\mathrm{e}}) f_{\Gamma_{\mathrm{e}}}(\gamma_{\mathrm{e}}) F_{\Gamma_{\mathrm{b}}}(\gamma_{\mathrm{e}})\,\mathrm{d}\gamma_{\mathrm{e}}\right]\\ &\quad - \frac{1}{D\ln 2}\left[\int_0^{\infty} \ln(1 + \gamma_{\mathrm{e}}) f_{\Gamma_{\mathrm{e}}}(\gamma_{\mathrm{e}})\,\mathrm{d}\gamma_{\mathrm{e}}\right]\\ &= \frac{1}{D\ln 2}[H_1 + H_2 - H_3],\end{aligned} \tag{33}$$

where H_1, H_2, and H_3 are shown as

$$\begin{aligned}H_1 &= \int_0^{\infty} \ln(1 + \gamma_{\mathrm{b}}) f_{\Gamma_{\mathrm{b}}}(\gamma_{\mathrm{b}}) F_{\Gamma_{\mathrm{e}}}(\gamma_{\mathrm{b}})\,\mathrm{d}\gamma_{\mathrm{b}}\\ &= \int_0^{\infty} \ln(1 + \gamma_{\mathrm{b}}) \sum_{l=0}^{L_{\mathrm{b}}-1} \frac{\sigma_{\mathrm{b}}^2 K_l}{P_X\sigma_{\mathrm{b},l}^2}\exp\left(-\frac{\sigma_{\mathrm{b}}^2}{P_X\sigma_{\mathrm{b},l}^2}\gamma_{\mathrm{b}}\right)\\ &\quad \times\left(1 - \exp\left(-\frac{\sigma_{\mathrm{e}}^2}{2\sigma^2 P_X}\gamma_{\mathrm{b}}\right)\right)\mathrm{d}\gamma_{\mathrm{b}}\\ &= \sum_{l=0}^{L_{\mathrm{b}}-1} K_l\left(\int_0^{\infty} \ln(1 + \gamma_{\mathrm{b}})\frac{\sigma_{\mathrm{b}}^2}{P_X\sigma_{\mathrm{b},l}^2}\exp\left(-\frac{\sigma_{\mathrm{b}}^2}{P_X\sigma_{\mathrm{b},l}^2}\gamma_{\mathrm{b}}\right)\mathrm{d}\gamma_{\mathrm{b}}\right.\\ &\quad \left. - \int_0^{\infty} \ln(1 + \gamma_{\mathrm{b}})\frac{\sigma_{\mathrm{b}}^2}{P_X\sigma_{\mathrm{b},l}^2}\exp\left(-\left(\frac{\sigma_{\mathrm{b}}^2}{P_X\sigma_{\mathrm{b},l}^2} + \frac{\sigma_{\mathrm{e}}^2}{2\sigma^2 P_X}\right)\gamma_{\mathrm{b}}\right)\mathrm{d}\gamma_{\mathrm{b}}\right)\\ &= -\sum_{l=0}^{L_{\mathrm{b}}-1} K_l\left(\exp\left(\frac{\sigma_{\mathrm{b}}^2}{P_X\sigma_{\mathrm{b},l}^2}\right)E_{\mathrm{i}}\left(-\frac{\sigma_{\mathrm{b}}^2}{P_X\sigma_{\mathrm{b},l}^2}\right)\right.\\ &\quad + \frac{2\sigma^2\sigma_{\mathrm{b}}^2}{2\sigma^2\sigma_{\mathrm{b}}^2 + \sigma_{\mathrm{e}}^2\sigma_{\mathrm{b},l}^2}\exp\left(\frac{\sigma_{\mathrm{b}}^2}{P_X\sigma_{\mathrm{b},l}^2} + \frac{\sigma_{\mathrm{e}}^2}{2\sigma^2 P_X}\right)\\ &\quad \left. \times E_{\mathrm{i}}\left(-\left(\frac{\sigma_{\mathrm{b}}^2}{P_X\sigma_{\mathrm{b},l}^2} + \frac{\sigma_{\mathrm{e}}^2}{2\sigma^2 P_X}\right)\right)\right),\end{aligned} \tag{34}$$

$$\begin{aligned}H_2 &= \int_0^{\infty} \ln(1 + \gamma_{\mathrm{e}}) f_{\Gamma_{\mathrm{e}}}(\gamma_{\mathrm{e}}) F_{\Gamma_{\mathrm{b}}}(\gamma_{\mathrm{e}})\,\mathrm{d}\gamma_{\mathrm{e}}\\ &= \int_0^{\infty} \ln(1 + \gamma_{\mathrm{e}})\frac{\sigma_{\mathrm{e}}^2}{2\sigma^2 P_X}\exp\left(-\frac{\sigma_{\mathrm{e}}^2}{2\sigma^2 P_X}\gamma_{\mathrm{e}}\right)\\ &\quad \times \sum_{l=0}^{L_{\mathrm{b}}-1} K_l\left[1 - \exp\left(-\frac{\sigma_{\mathrm{b}}^2}{P_X\sigma_{\mathrm{b},l}^2}\gamma_{\mathrm{e}}\right)\right]\mathrm{d}\gamma_{\mathrm{e}}\\ &= -\sum_{l=0}^{L_{\mathrm{b}}-1} K_l\left(\exp\left(\frac{\sigma_{\mathrm{e}}^2}{2\sigma^2 P_X}\right)E_{\mathrm{i}}\left(-\frac{\sigma_{\mathrm{e}}^2}{2\sigma^2 P_X}\right) + \frac{\sigma_{\mathrm{e}}^2\sigma_{b,l}^2}{2\sigma^2\sigma_b^2 + \sigma_{\mathrm{e}}^2\sigma_{b,l}^2}\right.\\ &\quad \left. \times\exp\left(\frac{\sigma_{\mathrm{e}}^2}{2\sigma^2 P_X} + \frac{\sigma_{\mathrm{b}}^2}{P_X\sigma_{\mathrm{b},l}^2}\right)E_{\mathrm{i}}\left(-\left(\frac{\sigma_{\mathrm{e}}^2}{2\sigma^2 P_X} + \frac{\sigma_{\mathrm{b}}^2}{P_X\sigma_{\mathrm{b},l}^2}\right)\right)\right),\end{aligned} \tag{35}$$

$$\begin{aligned}H_3 &= \int_0^{\infty} \ln(1 + \gamma_{\mathrm{e}}) f_{\Gamma_{\mathrm{e}}}(\gamma_{\mathrm{e}})\,\mathrm{d}\gamma_{\mathrm{e}}\\ &= \int_0^{\infty} \ln(1 + \gamma_{\mathrm{e}})\frac{\sigma_{\mathrm{e}}^2}{2\sigma^2 P_X}\exp\left(-\frac{\sigma_{\mathrm{e}}^2}{2\sigma^2 P_X}\gamma_{\mathrm{e}}\right)\mathrm{d}\gamma_{\mathrm{e}}\\ &= -\exp\left(\frac{\sigma_{\mathrm{e}}^2}{2\sigma^2 P_X}\right)E_{\mathrm{i}}\left(-\frac{\sigma_{\mathrm{e}}^2}{2\sigma^2 P_X}\gamma_{\mathrm{e}}\right).\end{aligned} \tag{36}$$

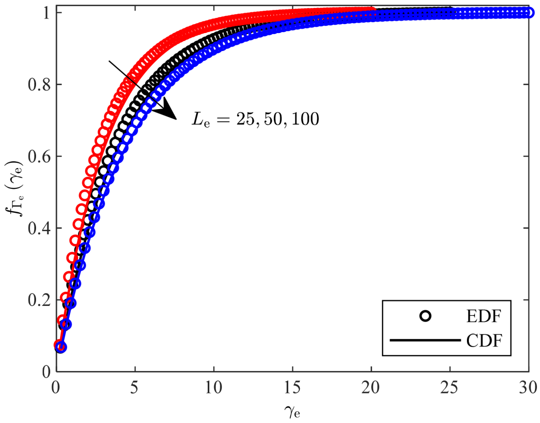

Fig. 3 *CDF of SNR of Eve*

3.4 Bit error rate (BER)

For BPSK modulation, the instantaneous BER expressions of Bob and Eve can be represented as [33]

$$P^{(m)}(\gamma_m) = Q(\sqrt{2\gamma_m}), \tag{37}$$

where

$$Q(t) = \int_t^{\infty} \frac{1}{\sqrt{2\pi}} \exp\left(-\frac{s^2}{2}\right) \mathrm{d}s = \frac{1}{\pi} \int_0^{\pi/2} \exp\left(-\frac{t^2}{2\sin^2\theta}\right) \mathrm{d}\theta$$

is one-dimensional Gaussian Q-function.

The expressions of the average BERs of Bob and Eve over fading channels can be written as

$$\bar{P}^{(m)} = \int_0^{\infty} P^{(m)}(\gamma_m) f_{\Gamma_m}(\gamma_m)\, \mathrm{d}\gamma_m. \tag{38}$$

Therefore, the average BER of Bob in the TR system is derived as (see (39)) . Similarly, the average BER of Eve can be derived as

$$\begin{aligned}\bar{P}^{(e)} &= \int_0^{\infty} P^{(e)}(\gamma_e) f_{\Gamma_e}(\gamma_e)\, \mathrm{d}\gamma_e \\ &= \int_0^{\infty} Q(\sqrt{2\gamma_e}) f_{\Gamma_e}(\gamma_e)\, \mathrm{d}\gamma_e \\ &= \int_0^{\infty} \left(\frac{1}{\pi} \int_0^{\pi/2} \exp\left(-\frac{\gamma_e}{\sin^2\theta}\right) \mathrm{d}\theta \right) \left(\frac{\sigma_e^2}{2\sigma^2 P_X} \exp\left(-\frac{\sigma_e^2}{2\sigma^2 P_X}\gamma_e\right) \right) \mathrm{d}\gamma_e \\ &= \frac{1}{\pi} \int_0^{\pi/2} \left(\frac{1}{\sin^2\theta} + \frac{\sigma_e^2}{2\sigma^2 P_X} \right)^{-1} \mathrm{d}\theta \\ &= \frac{1}{2}\left(1 - \sqrt{\frac{2\sigma^2 P_X}{2\sigma^2 P_X + \sigma_e^2}}\right).\end{aligned} \tag{40}$$

4 Simulation results

This section verifies the results of the theoretical analysis through simulation. The simulation environment is the same as the simulation of CDFs in Sections 3.1 and 3.2, i.e. the bandwidth is set as $B = 100$, 50, or 25 MHz and the corresponding number of paths is $L_b = 100$, 50, or 25.

The simulation results of the capacities of the legitimate channel are given in Fig. 4. To show the deviation of performance when ISI is neglected, the average capacities based, respectively, on SINR and SNR are simulated under different up-sampling factor D. For each channel realisation, the instantaneous signal and the ISI power of Bob are first calculated according to (9) and (10). Then SNR and SINR are calculated, respectively. The capacities of the legitimate channel are calculated according to the channel capacity formula, respectively, based on SNR and SINR. Fig. 4*a* plots the average values of the capacities based on SINR and SNR of the legitimate channel, respectively, when the up-sampling factors are $D = 1$, 10, 25, and 50 and the number of paths is $L_b =$ 100. Moreover, the simulation and theoretical values of the capacities are plotted in Fig. 4*b*, when the up-sampling factors are $D = 1$, 5, 10, and 25 and the number of paths is $L_b = 50$. Simultaneously, the capacities are shown in Fig. 4*c* when $L_b = 25$ and $D = 1$, 5, and 12. The theoretical values of ergodic capacities which are calculated according to (30) are plotted with unmarked solid lines. The y-axis is $D \times \bar{C}$, i.e. the D times of ergodic capacity. Since the value of D has no impact on the signal power, so SNR does not change when D is changing if other parameters keep the same. The theoretical ergodic capacity is derived on the basis of the PDF of SNR, so $D \times \bar{C}_b$ does not change with D. As a result, only one theoretical curve is drawn in the figures. From Fig. 4*a*, it can be found that the simulation values of the D times of the capacities based on SINR and SNR are very close to each other when $D = 25$, and they are almost coincident when $D = 50$. Similarly, the simulation values of the D times of the capacities based on SINR and SNR are almost coincident when $D = 25$ in Fig. 4*b*, and there are the same results in Fig. 4*c* when $D = 12$. The theoretical values are consistent with the simulation values based on SNR in all three numbers of paths, which prove that the derivation of the ergodic capacity of the legitimate channel is correct. Both signal power and ISI power increase proportionally with the increase of transmission power, so the numerator and denominator in the SINR expression increase synchronously, and the growth in SINR is not obvious with the increase of the transmission power. The SINR will approach a constant when the transmission power approaches infinity, so the capacity approached a constant too. The ISI power decreases as D increases and SINR is improved. So, $D \times \bar{C}_b$ has an upper bound, and the bound increases as D increases. $D \times \bar{C}_b$ has no upper bound in the simulation when $D = L_b/2$, which means that the ISI has almost completely eliminated. These show that the quality of the received signal can be improved by reducing spectral efficiency.

Fig. 5 plots the ergodic capacities of the wiretap channel when $L_e = 100$, 50, and 25, respectively. The parameters of the channel in the simulation are the same as those in the simulation of the

$$\begin{aligned}\bar{P}^{(b)} &= \int_0^{\infty} P^{(b)}(\gamma_b) f_{\Gamma_b}(\gamma_b)\, \mathrm{d}\gamma_b \\ &= \int_0^{\infty} Q(\sqrt{2\gamma_b}) f_{\Gamma_b}(\gamma_b)\, \mathrm{d}\gamma_b \\ &= \int_0^{\infty} \left(\frac{1}{\pi} \int_0^{\pi/2} \exp\left(-\frac{\gamma_b}{\sin^2\theta}\right) \mathrm{d}\theta \right) \left(\sum_{l=0}^{L_b-1} \frac{\sigma_b^2 K_l}{P_X \sigma_{b,l}^2} \exp\left(-\frac{\sigma_b^2}{P_X \sigma_{b,l}^2}\gamma_b\right) \right) \mathrm{d}\gamma_b \\ &= \frac{1}{\pi} \sum_{l=0}^{L_b-1} \frac{\sigma_b^2 K_l}{P_X \sigma_{b,l}^2} \int_0^{\pi/2} \left(\frac{1}{\sin^2\theta} + \frac{\sigma_b^2}{P_X \sigma_{b,l}^2} \right)^{-1} \mathrm{d}\theta \\ &= \frac{1}{2} \sum_{l=0}^{L_b-1} K_l \left(1 - \sqrt{\frac{P_X \sigma_{b,l}^2}{P_X \sigma_{b,l}^2 + \sigma_b^2}}\right).\end{aligned} \tag{39}$$

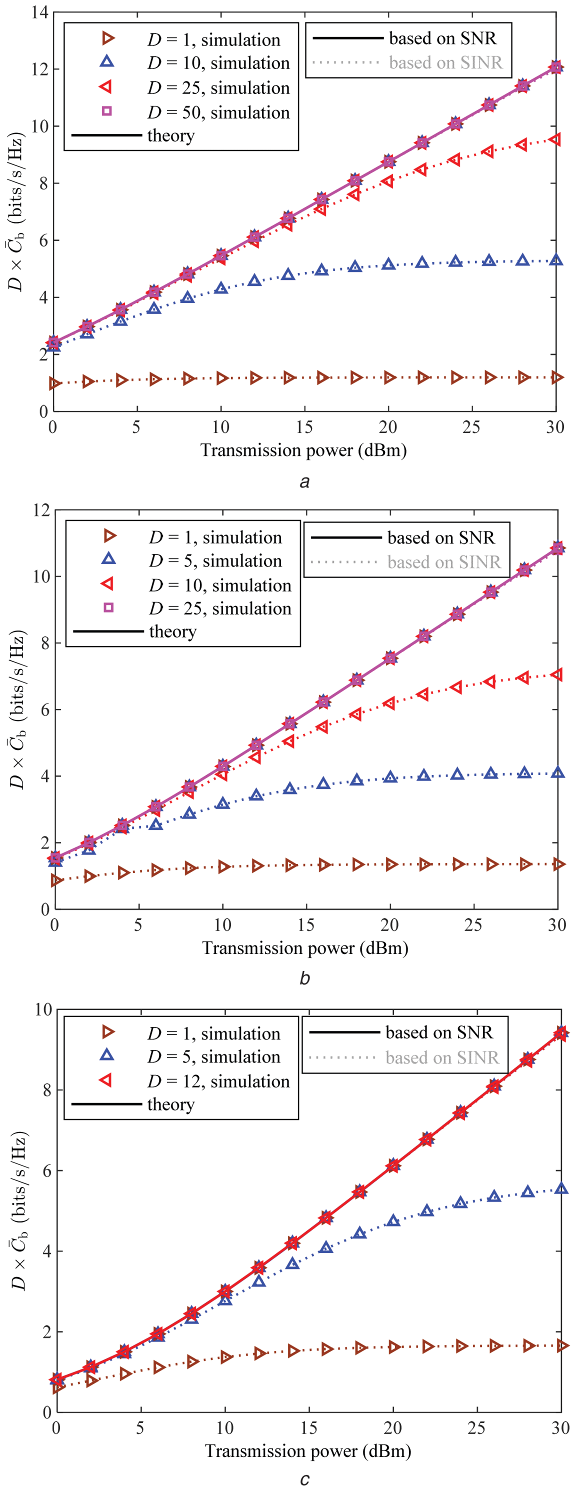

Fig. 4 *Ergodic capacity of the legitimate channel*
(a) $L_b = 100$, ***(b)*** $L_b = 50$, ***(c)*** $L_b = 25$

legitimate channel capacity. When $L_e = 100$ and $D = 50$, the simulation values based on SNR and SINR are very close to the theoretical values calculated according to (31). The theoretic values are slightly higher than the simulation values. There are similar results when $L_e = 50$ and $D = 25$, and it is true when $L_e = 25$ and $D = 12$. It can be seen that the deviation when $L_e = 100$ is smaller than those when $L_e = 50$ and 25. These further prove the feasibility of taking R and Q in (23) approximately as Gaussian random variables and the derivation of the capacity of the wiretap channel is acceptable. Moreover, the more the number of paths is, the smaller the deviation caused by the approximation is. It can be found that the capacity of the wiretap channel does not increase significantly when the number of paths increases.

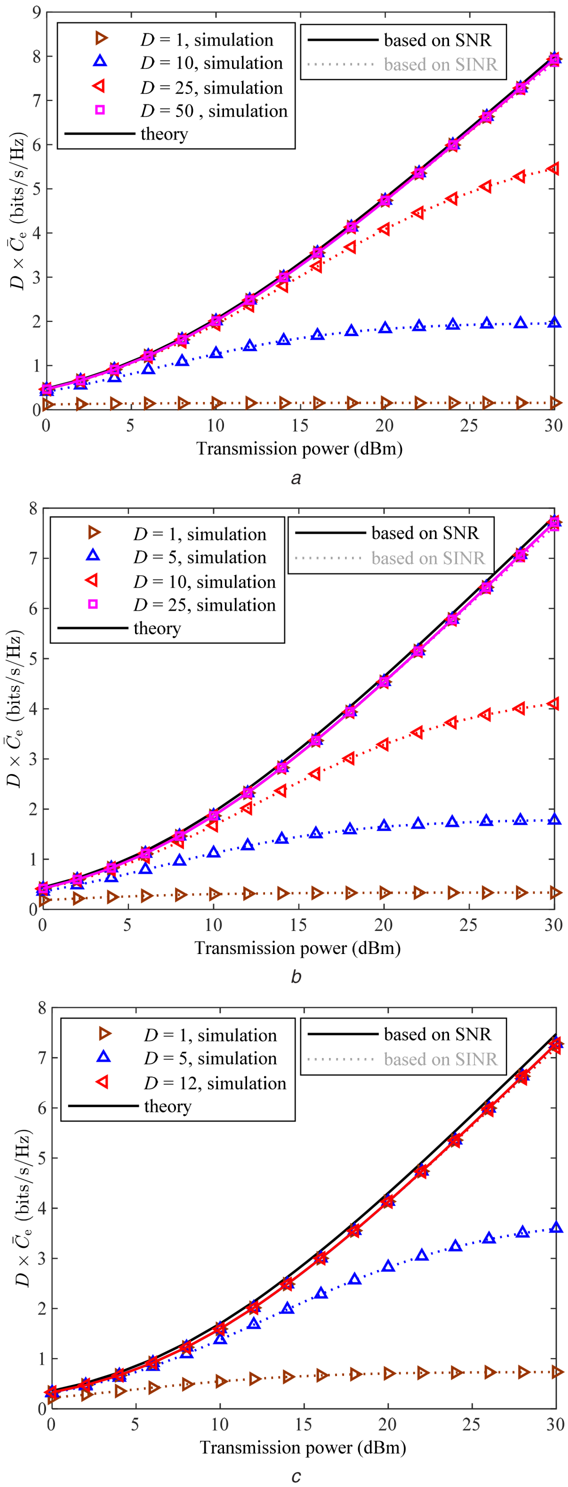

Fig. 5 *Ergodic capacity of the wiretap channel*
(a) $L_e = 100$, ***(b)*** $L_e = 50$, ***(c)*** $L_e = 25$

Fig. 6 plots the average values of the secrecy rate under different numbers of paths and up-sampling factors. The theoretical values of the ergodic secrecy rates are calculated according to (33) and they are plotted with unmarked solid lines. Similar to the simulations of capacity, the simulation values of secrecy rates based on both SNR and SINR are given. For the simulation values of the secrecy rate, the instantaneous capacities of the legitimate channel C_b and that of the wiretap channel C_e are calculated firstly for each channel realisation based on SINR or SNR, and then the secrecy rates are calculated according to the formula as follows:

$$R_s = [C_b - C_e]^+ \tag{41}$$

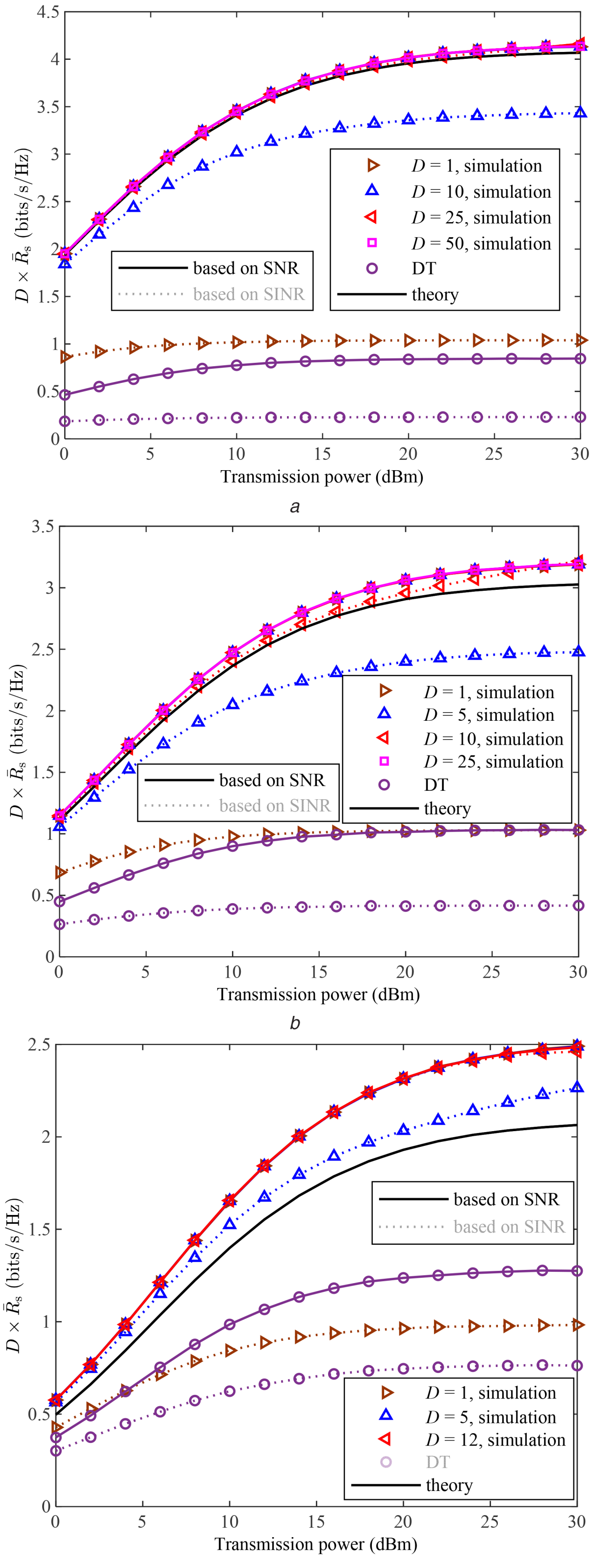

Fig. 6 *Ergodic achievable secrecy rate*
(a) $L_b = L_e = 100$, ***(b)*** $L_b = L_e = 50$, ***(c)*** $L_b = L_e = 25$

The average values are obtained by averaging the instantaneous secrecy rates among all channel realisations. It can be seen that the simulation values of secrecy rates based on SNR and SINR are almost coincident when $D = 50$ for $L_b = L_e = 100$, $D = 25$ for $L_b = L_e = 50$, and $D = 12$ for $L_b = L_e = 25$. The results indicate that the neglect of ISI in the performance analysis is feasible when D is large enough. The theoretical values are smaller than the simulation values. The difference decreases as the number of paths increases, and it is very small when $L_b = L_e = 100$. The difference is caused by the approximation in the derivation of the PDF of Eve's SNR. In the meantime, as the number of paths increases, the ergodic secrecy rate also increases. This is because the capacity of the legitimate channel is significantly improved when the number of paths increases, while there is no significant increase in the wiretap channel. Furthermore, the capacity of the legitimate channel is higher than that of the wiretap channel under the same number of paths and transmission power, which proves that TR can help to achieve secrecy transmission on the physical layer.

We also give the simulation results of a DT system for comparison when ISI is completely cancelled or is not cancelled, which are plotted with a solid line and a dotted line, respectively, in Fig. 6. The results show that the ergodic secrecy rate of the DT system almost does not increase with the increase of the transmission power if the ISI is not cancelled. Even if the ISI can be completely cancelled, the ergodic secrecy rate of the DT system only increases slightly with the increase of the transmission power in the low power region, and it does not increase in the high-power region. A non-zero instantaneous ergodic rate is obtained when the instantaneous capacity of the legitimate channel is greater than that of the wiretap channel, whereas the instantaneous ergodic rate becomes zero under the opposite condition. Owing to the random variation of the channel, the DT system can obtain a small ergodic secrecy rate even though the performances of the legitimate channel and the wiretap channel are the same in the simulation. Since the received SNRs (or SINRs) of Bob and Eve increase simultaneously when the transmission power is increasing, so the ergodic secrecy rate of the DT system does not increase proportionally with the increase of the transmission power, especially when ISI is not cancelled. It can be seen that the TR system has an obviously better security performance than that of the DT system.

With the increase of transmission power, the increase of $D \times \bar{R}_s$ is faster when D is larger than that when D is smaller, and the ceiling of the secrecy rate is higher too, which means that a higher value of $D \times \bar{R}_s$ can be obtained by properly reducing spectral efficiency. What is more, the $D \times \bar{R}_s$ for $D = 25$ and 50 when the number of paths is 100 and are also equal, and so are for $D = 10$ and 25 when the number of paths is 50. So D should not be set to higher than the one-quarter of the number of paths, because the secrecy performance is no longer improved by decreasing spectral efficiency when D is bigger enough. The $D \times \bar{R}_s$ can increase with the increase of the transmission power, but it has a ceiling, i.e. the $D \times \bar{R}_s$ has a limit value even if the transmission power increases to infinite. $D \times \bar{R}_s$ has a different feature to $D \times \bar{C}$, since the latter can keep increasing with the increase of the transmission power as long as D is big enough.

Finally, we present the BERs of Bob and Eve when BPSK modulation is used in Fig. 7, respectively, when the numbers of paths are $L_b = L_e = 100$, 50, and 25. Fig. 7*a* shows the simulation values of the average BERs of Bob and Eve when $L_b = L_e = 100$ and $D = 1$, 10, 25, and 50. The simulation results are shown in Fig. 7*b* when $L_b = L_e = 50$ and $D = 1$, 5, 10, and 25, and these are plotted in Fig. 7*c* when $L_b = L_e = 25$ and $D = 1$, 5 and 12. Simultaneously, the theoretical values of BER obtained according to (39) and (40) are plotted too. It can be seen that the simulation values of Bob are consistent with the theoretical values when $D =$ 25 and 50 in Fig. 7*a*, and it is also true when $D = 25$ in Fig. 7*b* or when $D = 12$ in Fig. 7*c*. The conclusion can be obtained that the simulation values of Bob's BER are in agreement with theoretical values when the up-sampling factor D is set to one half of the number of paths, which means that the ISI has been almost completely cancelled. However, it also can be found from Figs. 7*a–c* that the theoretical values of Eve's BER are slightly lower than the simulation values when D is half of the number of paths. The differences are caused by the approximation processing in the derivation of PDF of Eve's SNR, and it matches the fact that the curve of the theoretical CDF of SNR is slightly offset from the right to the curve of EDF in Fig. 3. The BERs of Eve are higher than those of Bob in all cases. As D increases, the BERs of Bob

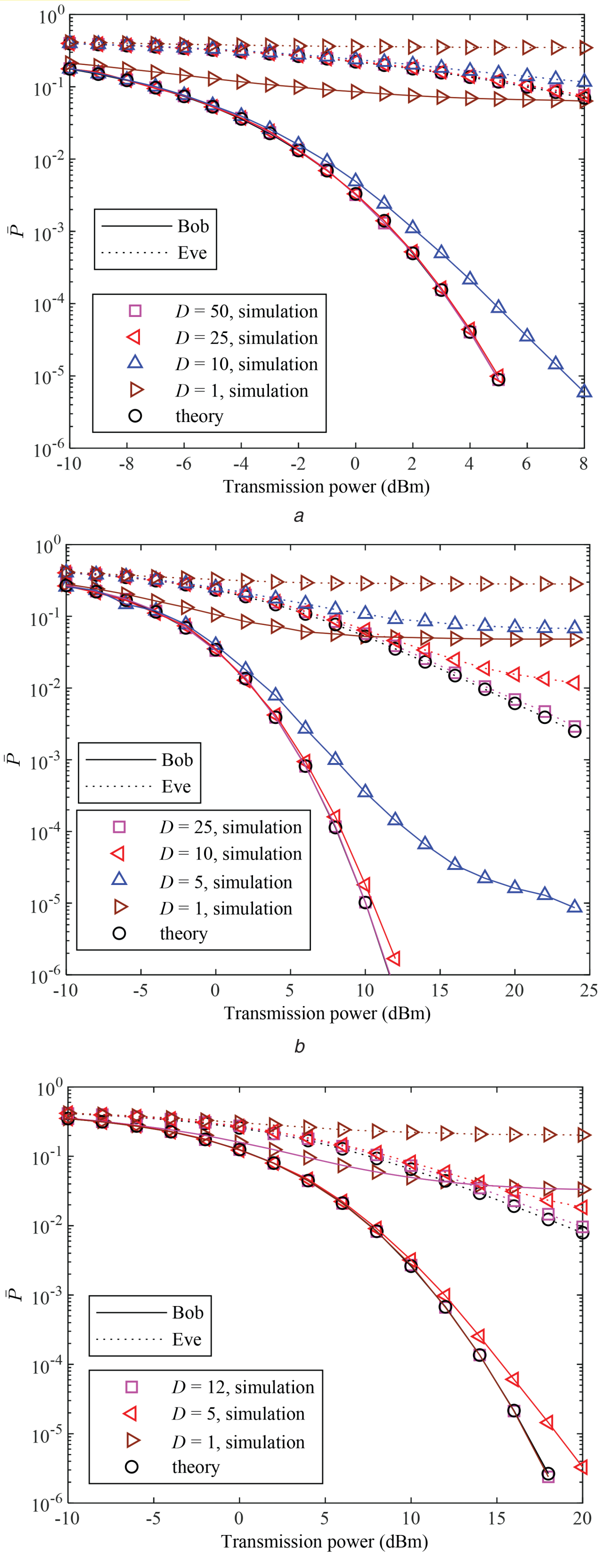

a

b

c

Fig. 7 *Bit error rates*
(a) $L_b = L_e = 100$, ***(b)*** $L_b = L_e = 50$, ***(c)*** $L_b = L_e = 25$

and Eve decrease owing to the decrease of ISI power. The BER of Bob declines exponentially along with the increase of transmission power P_X, while that of Eve declines very slowly. For example, from Fig. 7*a*, when P_X is 5 dBm and $D = 50$, Bob's BER is about 10^{-5}, while Eve's BER is 10^{-1}.

To compare the BER under a different number of paths, the BER curves of simulation for $D = 50$ in Fig. 7*a*, $D = 25$ in Fig. 7*b* and $D = 12$ in Fig. 7*c* are re-plotted in Fig. 8. It can be found that the BER of Bob decreases obviously as the number of paths increases, while the BER of Eve almost does not decrease. For example, Bob's BER can achieve 10^{-5} when the transmission power is about 16 dBm when the number of paths is 25. The required power decreases to 10 and 5 dBm when the number of paths increases to 50 and 100, respectively, to achieve the same BER. However, Eve's BER is basically not changed with the increase in the number of paths. The reason is explained as follows. The intended receiver, i.e. Bob, can obtain path diversity gain thanks to the TR pre-filtering. As the number of paths increases, the distribution of Bob's SNR shifts to the higher value area, i.e. the diversity gain increases. As a result, Bob's BER decreases quickly with the increase of transmission power, and the larger the number of paths is, the faster the rate of decline is. However, the unintended receiver, i.e. Eve, cannot obtain diversity gain, so the distribution of Eve's SNR concentrates in a low-value area, and does not shift obviously with the increase of the number of paths. So, Eve's BER decreases very slowly with the increase of transmission power, and it is significantly higher than Bob's BER. The large gap between the BERs of Bob and Eve means that secure transmission of information can be realised and increasing the number of paths can help to improve the security performance of the system. The increase in the number of paths can be achieved by using a broader bandwidth.

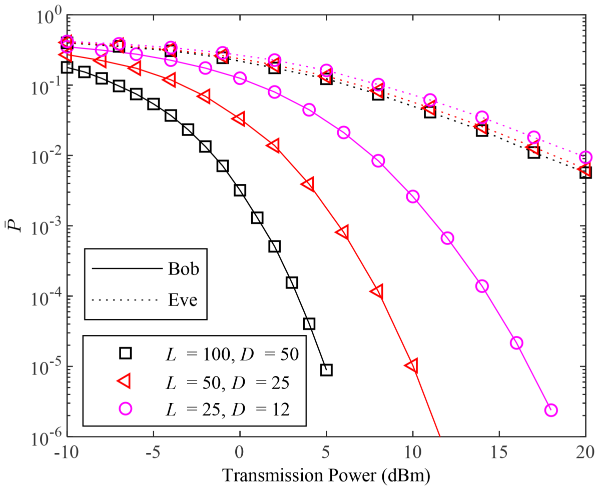

Fig. 8 *Comparison of BERs under different number of paths*

5 Conclusion

In this study, the PLS performance of the TR pre-coding system over the Rayleigh fading channel is analysed. The probability distribution of the received SNR of Eve is derived. Based on the derived PDF, and the PDF of received SNR of Bob given in [15], the theoretical values of the ergodic capacities of the legitimate channel and the wiretap channel and the ergodic secrecy rate are derived. What is more, the BERs of Bob and Eve are given when BPSK is used. Finally, the correctness of the theoretical analysis is verified through simulation. Through the simulation results, the following conclusions can be obtained. (i) The average SNR of Bob is significantly higher than that of Eve, so the capacity of the legitimate channel is significantly higher than the capacity of the wiretap channel. A high ergodic secrecy rate can be achieved. (ii) As the number of paths increases, a higher diversity gain can be obtained by Bob, so its average SNR increases and its BER decreases more quickly with the increase of the transmission power. However, the SNR of Eve does not increase significantly, and the BER is always decreasing slowly with the increase of transmission power. Therefore, the ergodic achievable secrecy rate increases and the security performance is improved. (iii) The larger is the value of up-sampling factor D, the smaller is the power of ISI at Bob. So Bob's BER decreases obviously, while Eve's BER basically does not decrease because its SINR does not increase obviously as D increases. Furthermore, D times of the ergodic achievable secrecy rate grow faster when D is larger than that when D is smaller. So a better secrecy performance can be obtained by properly reducing spectral efficiency. (iv) The ergodic achievable secrecy rate of the DT system quickly tends to a very low ceil as the transmission power increases, while the TR transmission system has a much higher ceil. So the TR system can achieve a better PLS performance than the DT system. However, it can be seen that simulation values of ergodic capacities and achievable secrecy rate based on the SINR are much lower than those based on the SNR and theoretic values when the up-sampling factor D is small. The difference between the simulation values and theoretic values of BER is obvious too in this case. The theoretic analysis of ergodic capacity, achievable secrecy rate, and BER are based on the probability distributions of the received SINR. Since the expression of SINR is very complicated and the components of the ISI and signal are not independent of each other, the probability distributions of the received SINR of Bob and Eve have not been derived in this study. To get more accurate expressions of PLS performance, the probability distributions of the received SINR of Bob and Eve should be derived first, which is a challenging and important work in future research. By using the TR technique, TRDMA can be realised. However, the non-orthogonal multiple access (NOMA) has the potential to achieve the object of the massive connects in 5G networks. The TR technique can be employed in NOMA networks to enhance system performance. Similar to the work of Xiang *et al*. [34], using the TR technique to improve the PLS performance of NOMA networks will be a valuable job.

6 Acknowledgments

This work was supported by The National Natural Science Foundation of China under grant nos. 61971080 and 61471076, the Chongqing Research Program of Basic Research and Frontier Exploration under grant no. cstc2018jcyjAX0432, and The Key Project of Science and Technology Research of Chongqing Education Commission under grant nos. KJZD-K201800603 and KJZD-M201900602. The authors would like to thank the anonymous reviewers as well as the editors for their excellent feedback, which is of great help in improving the quality of this paper.

7 References

[1] Chen, Y., Wang, B., Han, Y.*,* *et al.*: 'Why time reversal for future 5G wireless?', *IEEE Signal Process. Mag.*, 2016, **33**, (2), pp. 17–26

[2] Chen, Y., Yang, Y.H., Han, F., *et al.*: 'Time-reversal wideband communications', *IEEE Signal Process. Lett.*, 2013, **20**, (12), pp. 1219–1222

[3] Nguyen, H.T., Kovacs, I.Z., Eggers, P.C.F.: 'A time reversal transmission approach for multiuser UWB communications', *IEEE Trans. Antennas Propag.*, 2006, **54**, (11), pp. 3216–3224

[4] Xu, Q., Jiang, C., Han, Y., *et al.*: 'Waveforming: an overview with beamforming', *IEEE Commun. Surv. Tutor.*, 2018, **20**, (1), pp. 132–149

[5] Han, Y., Chen, Y., Wang, B.B.*,* *et al.*: 'Time-reversal, massive multipath effect: a single-antenna 'massive MIMO' solution'. *IEEE Trans. Commun.*, 2016, **64**, (8), pp. 3382–3394

[6] Fink, M.: 'Time reversal of ultrasonic fields. I. Basic principles', *IEEE Trans. Ultrason., Ferroelectr., Freq. Control*, 1992, **39**, (5), pp. 555–566

[7] Derode, A., Roux, P., Fink, M.: 'Robust acoustic time reversal with high-order multiple scattering', *Phys. Rev. Lett.*, 1995, **75**, (23), pp. 4206–4209

[8] Bouzigues, M.A., Siaud, I., Helard, M.*,* *et al.*: 'Turn back the clock: time reversal for green radio communications', *IEEE Veh. Technol. Mag.*, 2013, **8**, (1), pp. 49–56

[9] Fromenteze, T., Carsenat, D., Decroze, C.: 'A precorrection method for passive UWB time-reversal beamformer', *IEEE Antennas Wirel. Propag. Lett.*, 2013, **12**, pp. 836–840

[10] Li, Y., Xia, M.: 'Time reversal imaging based on synchronism', *IEEE Antennas Wirel. Propag. Lett.*, 2017, **16**, pp. 2058–2061

[11] Wu, Z.H., Han, Y., Chen, Y.*,* *et al.*: 'A time-reversal paradigm for indoor positioning system', *IEEE Trans. Veh. Technol.*, 2015, **64**, (4), pp. 1331–1339

[12] Cozza, A., Monsef, F.: 'Steering focusing waves in a reverberation chamber with generalized time reversal', *IEEE Trans. Antennas Propag.*, 2017, **65**, (3), pp. 1349–1356

[13] Wang, B.B., Wu, Y.L., Han, F.*,* *et al.*: 'Green wireless communications: a time-reversal paradigm', *IEEE J. Sel. Areas Commun.*, 2011, **29**, (8), pp. 1698–1710

[14] Han, F., Yang, Y.H., Wang, B.*,* *et al.*: 'Time-reversal division multiple access over multi-path channels', *IEEE Trans. Commun.*, 2012, **60**, (7), pp. 1953–1965

[15] Lei, W., Yao, L.: 'On the performance of time reversal communication systems', *IEEE Commun. Lett.*, 2019, **23**, (4), pp. 680–683

[16] Wyner, A.D.: 'The wire-tap channel', *Bell Syst. Tech. J.*, 1975, **54**, (8), pp. 1355–1387

[17] Yang, T., Zhang, R., Cheng, X.*,* *et al.*: 'Secure massive MIMO under imperfect CSI: performance analysis and channel prediction', *IEEE Trans Inf. Forensics Sec.*, 2019, **14**, (6), pp. 1610–1623

[18] Zhang, R., Cheng, X., Yang, L.: 'Cooperation via spectrum sharing for physical layer security in device-to-device communications underlaying cellular networks', *IEEE Trans. Wirel. Commun.*, 2016, **15**, (8), pp. 5651–5663

[19] Cao, W., Lei, J., Liu, W.*,* *et al.*: 'Secure performance of time reversal precoding technique in MISO OFDM systems'. Communications Security Conf. (CSC), Beijing, China, May 2014, pp. 1–5

[20] Tan, V.T., Ha, D.B., Tran, D.D.: 'Evaluation of physical layer secrecy in MIMO ultra-wideband system using time-reversal techniques'. Int. Conf. on Computing, Management and Telecommunications (ComManTel), Da Nang, Vietnam, April 2014, pp. 70–74

[21] El-Sallabi, H., Aldosari, A.: 'Characterization of secrecy capacity of time reversal technique for wireless physical layer security'. Int. Symp. on Wireless Personal Multimedia Communications (WPMC), Shenzhen China, November 2016, pp. 194–198

[22] Tran, H.V., Tran, H., Kaddoum, G.*,* *et al.*: 'Effective secrecy-SINR analysis of time reversal-employed systems over correlated multi-path channel'. IEEE 11th Int. Conf. on Wireless and Mobile Computing, Networking and Communications (WiMob), Abu Dhabi, United Arab Emirates, October 2015, pp. 527–532

[23] Wang, L., Li, R., Cao, C.*,* *et al.*: 'SNR analysis of time reversal signaling on target and unintended receivers in distributed transmission', *IEEE Trans. Commun.*, 2016, **64**, (5), pp. 2176–2191

[24] Li, S., Li, N., Tao, X.F.*,* *et al.*: 'Artificial noise inserted secure communication in time-reversal systems'. IEEE Wireless Communications and Networking Conf. (WCNC), Barcelona, Spain, April 2018, pp. 1–6

[25] Tran, H.V., Kaddoum, G., Tran, H.*,* *et al.*: 'Time reversal SWIPT networks with an active eavesdropper: SER-energy region analysis'. IEEE 84th Vehicular Technology Conf. (VTC), Montreal, QC, Canada, September 2016, pp. 1–5

[26] He, B.Y., Sun, T., Wang, Z.*,* *et al.*: 'A fine-grained analysis of time reversal MU-MISO systems over correlated multipath channels with imperfect CSI', *IEEE Access*, 2018, **6**, pp. 69516–69527

[27] Viteri-Mera, C.A., Teixeira, F.L.: 'Equalized time reversal beamforming for frequency-selective indoor MISO channels', *IEEE Access*, 2017, **5**, pp. 3944–3957

[28] Zhou, C., Guo, N., Qiu, R.C.M.: 'Time-reversed ultra-wideband (UWB) multiple input multiple output (MIMO) based on measured spatial channels', *IEEE Trans. Veh. Technol.*, 2009, **58**, (6), pp. 2884–2898

[29] Simon, M.K.: '*Probability distributions involving Gaussian random variables*' (Springer Press, 2006)

[30] Grimmett, G.R., Stirzaker, D.R.: '*Probability and random processes*' (Oxford University Press, 2011, 3rd edn.)

[31] 'The expected value of the ratio of correlated random variables'. Available at https://www.depts.ttu.edu/biology/people/Faculty /Rice/home/ratio-derive.pdf, accessed 2009

[32] Gradshteyn, I.S., Ryzhik, I.M., Jeffrey, A.*,* *et al.*: '*Table of integrals, series, and products*' (Academic Press, 1980, 7th edn.)

[33] Simon, M.K., Alouini, M.S.: '*Digital communication over fading channels: a unified approach to performance analysis*' (John Wiley & Sons, Inc. Press, 2000)

[34] Xiang, Z., Yang, W., Pan, G.*,* *et al.*: 'Physical layer security in cognitive radio inspired NOMA network', *IEEE J. Sel. Top. Signal Process.*, 2019, **13**, (3), pp. 700–714